Macroscopic boundary effects in the one-dimensional extended Bose-Hubbard model

Sebastian Stumper* and Junichi Okamoto
Physikalisches Institut, Albert-Ludwigs-Universität Freiburg, Hermann-Herder-Straße 3, 79104 Freiburg, Germany

(Received 14 January 2020; revised manuscript received 16 April 2020; accepted 26 May 2020; published 23 June 2020)

We study the effect of different open boundary conditions on the insulating ground states of the one-dimensional extended Bose-Hubbard model at and near unit filling. To this end, we employ the density-matrix renormalization-group method with system sizes up to 250 sites. To characterize the system, various order parameters and entanglement entropies are calculated. When opposite edge potentials are added to the two ends of the chain, the inversion symmetry is explicitly broken, and the regular bulk phases appear. On the other hand, simple open boundary conditions often exhibit nondegenerate ground states with a domain wall in the middle of the chain, which induces a sign flip of an order parameter. Such a domain wall can lead to an algebraic behavior of the off diagonals of the single-particle density matrix. We show that this algebraic behavior adds only a finite contribution to the entanglement entropy, which does not diverge as the system size increases. Therefore, it is not an indication of a superfluid phase. We confirm this picture by analytical calculations based on an effective Hamiltonian for a domain wall.

DOI: 10.1103/PhysRevA.101.063626

I. INTRODUCTION

Cold atoms in optical lattices provide flexible experimental settings for implementing a large variety of many-body Hamiltonians. Due to the controllability of model parameters, a wealth of quantum phases has been created such as superfluids (SFs), Mott insulators, or Luttinger liquids [1]. The cold atom setups can also serve as quantum simulators for solid-state systems [2,3]. Although the on-site interaction in an optical lattice is usually dominant due to short-ranged *s*-wave interaction, it is possible to introduce long-ranged interactions, for instance by using dipolar magnetic atoms or Rydberg atoms [4,5].

One of the most studied models for long-ranged interactions includes an on-site and a nearest-neighbor interaction term. For bosonic particles it is called an extended Bose-Hubbard model (EBHM). In the strongly interacting regime, the model hosts various insulating phases such as a Mott insulator (MI) or a density wave (DW) phase [6]. In one dimension, the Haldane insulator (HI), an analog of the Haldane phase in antiferromagnetic spin-1 chains, appears [7–9]. This is a symmetry-protected topological phase [10], which cannot be distinguished from the MI based on any local order parameter. Rather the number fluctuations in the ground states of MI and HI display different patterns, which are detected by nonlocal correlation functions. The HI is expected to exhibit fractionally charged edge states, which makes it a particularly appealing object to study due to possible applications in quantum computing. Understanding and controlling the edge states is thus an important problem.

In this paper, we propose to use boundary conditions (BCs) as another means of controlling insulating ground states of the one-dimensional (1D) EBHM at or near unit filling. We consider various open boundary conditions, which we expect to be experimentally realizable. For example, local edge potentials can be accomplished by using optical tweezers [11]. The dependencies on the boundary conditions of order parameters and of the entanglement entropies are numerically studied by a density-matrix renormalization-group (DMRG) method based on matrix product states (MPSs) [12]. When opposite edge potentials are applied, the inversion symmetry of the model is explicitly broken, and the usual bulk phases are stable. However, as is often the case in classical systems [13], we find that several other boundary conditions lead to a formation of a domain wall in the system. It is shown that such a domain wall induces an algebraic behavior in the off-diagonal elements of the single-particle density matrix leading to an increase of the entanglement entropy. We find that the local effect of the domain wall on the ground-state properties is rather minor, while we expect that the dynamical properties are more prominently affected [14].

The 1D EBHM has been studied in many contexts. The ground-state phase diagram has been accurately mapped out by DMRG in Refs. [9,15], and also by quantum Monte Carlo [16–18]. Excitation spectrum and linear responses were studied in Refs. [14,19,20]. References [21,22] give a detailed analysis of entanglement entropies. A dependence of the bulk properties on the boundary conditions was considered in Ref. [23]. We revisit the variants of open boundary conditions considered therein and propose a simple effective picture to rationalize the numerical results. In particular, we argue that the entanglement entropy of a system with a domain wall does not diverge as the system size increases, and that it is not an indication of a bulk superfluid phase.

The remainder of the paper is organized as follows. In Sec. II, the model and observables of interest are introduced. Moreover, we discuss the relation to antiferromagnetic spin-1

*sebastian.stumper@physik.uni-freiburg.de

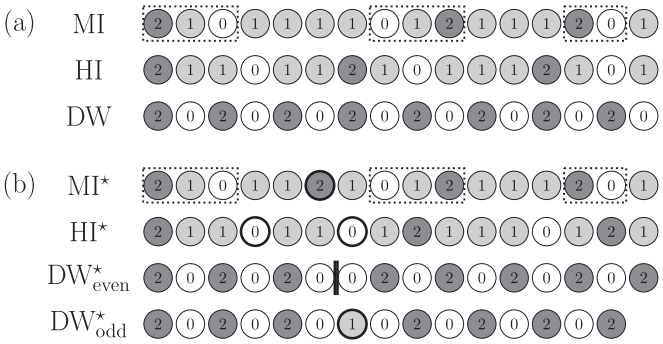

FIG. 1. (a) Fluctuations pattern in a state with parity order (MI) or string order (HI), along with density wave occupation pattern without fluctuations (DW). The HI exhibits a dilute density wave order $\ldots 2 \ldots 0 \ldots 2 \ldots 0 \ldots$, while the MI is characterized by bound doublon-holon pairs. (b) Single-particle-like defects (MI* and DW$^\star_{\text{odd}}$ [i.e., odd L]) and domain-wall-like defects (HI* and DW$^\star_{\text{even}}$ [i.e., even L]). In the HI and DW phases, the closest fluctuations to both edges are $\delta n = 1$. For the DW phase with even L and the HI, unit filling implies that there are two consecutive $\delta n = -1$ in the middle (thick circles).

chains and boundary conditions that we use. Section III is devoted to correlation functions and order parameters. These results are then put into perspective by further calculations of entanglement entropies in Sec. IV, followed by the conclusion in Sec. V. Technical aspects that are not covered in the main text are discussed in the Appendices.

II. MODEL

The Hamiltonian of the 1D EBHM on an open chain is given by

$$\hat{H} = -J \sum_{i=1}^{L-1} (\hat{a}_i^\dagger \hat{a}_{i+1} + \text{H.c.}) + \frac{U}{2} \sum_{i=1}^{L} \hat{n}_i(\hat{n}_i - 1) + V \sum_{i=1}^{L-1} \hat{n}_i \hat{n}_{i+1}, \tag{1}$$

where $\hat{a}_i^\dagger$ and $\hat{a}_i$ are bosonic creation and annihilation operators for site i and $\hat{n}_i$ denotes the corresponding number operator. The parameters J, U, and V represent the strength of hopping, on-site, and nearest-neighbor interaction, respectively. We focus on cases at or near unit filling factor $\overline{n} = N/L \simeq 1$ and set $J = 1$ in the remainder of the paper.

A. Observables

The quantum phases of the 1D EBHM are characterized by the density wave, string, parity, and superfluid correlation functions

$$\begin{aligned} C_{\text{DW}}(i,j) &= \langle \delta\hat{n}_i (-1)^i \delta\hat{n}_j (-1)^j \rangle, \\ C_{\text{str}}(i,j) &= \left\langle \delta\hat{n}_i (-1)^{\sum_{k=i}^{j-1} \delta\hat{n}_k} \delta\hat{n}_j \right\rangle, \\ C_{\text{par}}(i,j) &= \left\langle (-1)^{\sum_{k=i+1}^{j-1} \delta\hat{n}_k} \right\rangle, \\ C_{\text{SF}}(i,j) &= \langle \hat{a}_i^\dagger \hat{a}_j \rangle, \end{aligned} \tag{2}$$

where $\delta\hat{n}_i = \hat{n}_i - 1$. C_{DW} measures the local staggered density modulations, while C_{str} and C_{par} are nonlocal. The latter two can be illustrated by considering the limit of large $U \gg J$, where the local Hilbert spaces can be effectively reduced to occupation numbers $n = 0, 1, 2$. A nonvanishing string order indicates a density wave pattern in the number fluctuations [see Fig. 1(a)], where deviations from occupation number $n = 1$ alternate between $n = 0$ (holon) and 2 (doublon), but appear at arbitrary distances [8]. Similarly, parity order indicates the presence of spatially bound doublon-holon pairs where doublons and holons do not necessarily alternate [see Fig. 1(a)]. Finally, C_{SF} measures the off-diagonal (quasi-) long-range order of the single-particle density matrix [24], indicating a gapless superfluid phase.

The order parameters O_{DW}, O_{str}, and O_{par} are defined as the corresponding long-distance limits of correlation functions [7]

$$O = \lim_{|i-j|\to\infty} C(i,j). \tag{3}$$

One can identify the three gapped phases by these order parameters (see Table I): MI by $O_{\text{par}} \neq 0$ and $O_{\text{str}} = O_{\text{DW}} = 0$, the HI by $O_{\text{str}} \neq 0$ and $O_{\text{par}} = O_{\text{DW}} = 0$, and the DW phase by $O_{\text{str}} \neq 0 \neq O_{\text{DW}}$ (here C_{par} oscillates).

On the other hand, off-diagonal long-range order does not exist for the one-dimensional case, even with arbitrarily weak interactions. Instead, SF order is marked by an algebraic decay $C_{\text{SF}}(i,j) \sim |i-j|^{-K}$ [25,26]. Moreover, contrary to the gapped phases (MI, HI, and DW), the superfluid phase has gapless excitations. In one dimension, it behaves as a Tomonaga-Luttinger liquid, which is similar to critical modes near phase boundaries; both of them can be described by a conformal field theory. Such a critical behavior is reflected in the entanglement entropy. For any subsystem, the entanglement entropy is defined as the von Neumann entropy of the corresponding reduced density matrix. For a subsystem of size l that is the left block of a system of size L, we denote the entropy as $S_L(l)$. In this case, in a critical system, the entanglement entropy shows the following dependence on

TABLE I. Nonzero DW, string, and parity order parameters depending on V and for each boundary condition. The on-site interaction is set to $U = 6$ throughout. The superscript $\star$ indicates a sign flip in the corresponding correlation function, an illustration of which is depicted in Fig. 1.

	MI ($V \lesssim 3.5$)	HI ($3.5 \lesssim V \lesssim 3.9$)	DW ($V \gtrsim 3.9$)
(A even)	Parity	String*	DW* + string*
(A odd)	Parity	String*	DW + string*
(B)	Parity	String	DW + string
(C even)	Parity* ($V \lesssim 2.4$), parity ($V \gtrsim 2.4$)	String	DW* + string*

system and block size [27]:

$$S_L(l) = \frac{c}{6} \ln\left[\frac{2L}{\pi} \sin\left(\frac{\pi l}{L}\right)\right], \tag{4}$$

where c is the central charge of the underlying conformal field theory. In case of a Tomonaga-Luttinger liquid, $c = 1$ is expected. We will refer to the above formula to check whether certain boundary conditions can induce a SF phase.

B. Relation to the spin-1 model

As we have discussed in the introduction, the HI is an analog of the Haldane phase of antiferromagnetic spin-1 chains. Therefore, much of the common intuition about the strong-coupling regime of the 1D EBHM stems from an effective spin-1 model introduced by Dalla Torre *et al.* [7]. The effective spin model is obtained by restricting number fluctuations to $|\delta\hat{n}_i| \leqslant 1$ in the EBHM. By replacing $\delta\hat{n}_i \to S_i^z$ and $\hat{a}_i^{(\dagger)} \to \hat{S}_i^{-(+)}$, we find

$$\hat{H}_{\text{spin}} = \sum_i \left(\hat{S}_i^x \hat{S}_{i+1}^x + \hat{S}_i^y \hat{S}_{i+1}^y + \Delta \hat{S}_i^z \hat{S}_{i+1}^z\right) + D \sum_i \left(\hat{S}_i^z\right)^2, \tag{5}$$

where we have defined $\Delta = V/2J$ and $D = U/4J$. Setting the total magnetization to $\sum_i \langle \hat{S}_i^z \rangle = 0$ is equivalent to unit filling in the 1D EBHM. For $D, \Delta \gg 1$, there exist three phases analogous to those of the 1D EBHM. These are defined by order parameters obtained from Eq. (2) by substituting $\hat{S}_i^z$ for $\delta\hat{n}_i$ (we do not consider the components $\hat{S}^x$ and $\hat{S}^y$ here). The MI corresponds to a large-D phase in the limit $D \gg \Delta$, the DW phase corresponds to a Néel phase in the opposite limit $\Delta \gg D$, and the HI corresponds to the Haldane phase in the intermediate regime where $D \sim \Delta$ [28].

The ground states of the Haldane and Néel phases in an open chain show broken symmetries. More precisely, Kennedy and Tasaki showed that a so-called hidden $\mathbb{Z}_2 \times \mathbb{Z}_2$ symmetry is broken in the Haldane phase [29]. According to the valence-bond picture introduced by Affleck *et al.* [30], this corresponds to four degenerate configurations of effective spin-1/2 degrees of freedom at the two edges. The Néel phase holds a broken $\mathbb{Z}_2$ symmetry of spin flips $\hat{S}_i^z \leftrightarrow -\hat{S}_i^z$; in case of the open chain with even L, this is equivalent to broken lattice inversion symmetry.

Naively thinking, the ground states of corresponding phases in the 1D EBHM show similar degeneracies. For example, one might expect a broken lattice inversion symmetry in the DW phase (a particle-hole symmetry corresponding to the spin flips is obviously not present). We note, however, that the open boundary condition prohibits such degeneracy. This is because the nearest-neighbor term of the 1D EBHM requires additional local magnetic fields of strength Δ at the edges in the effective model

$$\begin{aligned}\sum_{i=1}^{L-1} \hat{n}_i \hat{n}_{i+1} &= \sum_{i=1}^{L-1} (\delta\hat{n}_i \delta\hat{n}_{i+1} + \hat{n}_i + \hat{n}_{i+1} - 1) \\ &\to \sum_{i=1}^{L-1} \hat{S}_i^z \hat{S}_{i+1}^z - \hat{S}_1^z - \hat{S}_L^z + \text{const.}\end{aligned} \tag{6}$$

Therefore, both the hidden $\mathbb{Z}_2 \times \mathbb{Z}_2$ symmetry and spin-flip symmetry are not present in the effective Hamiltonian, while lattice inversion symmetry survives. We will see that the edge fields of Eq. (6) have the effect of pinning the edge spins, preventing a breaking of the remaining inversion symmetry.

C. Boundary conditions

As our discussion in the previous subsection indicates, a specific choice of boundary conditions can influence the ground state significantly. It is thus important to know how the bulk phases depend on the local boundary conditions. Experimentally, different boundary conditions might be chosen as an extra tuning knob to control quantum states.

In the present paper we study an open chain of Eq. (1) with the following boundary conditions and filling factors [21,23]: (A) $\overline{n} = 1$ and no further conditions; (B) $\overline{n} = 1$ and opposite chemical potentials at the left and right edge sites—$\mu(\hat{n}_1 - \hat{n}_L)$ with $\mu = 2J$; and (C) one extra boson $N = L + 1$ (which implies $\overline{n} \to 1$ for $L \to \infty$) and no further conditions. The open boundary condition (A) in the 1D EBHM corresponds to extra magnetic fields at the edges in the spin-1 model as shown in Eq. (6). Originally, (B) and (C) were meant to lift ground-state degeneracies in the spin-1 model. First, we note that the edge potentials of (B) are substantially larger than what would be needed to numerically choose one of two degenerate ground states which break inversion symmetry. In the corresponding spin-1 model, this is necessary to overcome the pinning effect of the attractive edge potentials of Eq. (6). Alternatively one may explicitly compensate the attractive edge potentials by applying symmetric potentials of strength V. However, even in this case, small asymmetric edge fields are necessary for convergence to a unique ground state. As we found the effect of this variant to be very similar to (B), we do not further consider it. Second, the idea behind the extra boson in (C) is that it localizes close to the edges in the HI phase, contributing an effective magnetization of $m = 1/2$ on each side [21]. With weak nearest-neighbor interaction, however, such an extra particle may not be localized at the edges, and forms a domain-wall-like excitation in the middle of the chain (see Sec. III).

In the following sections, we closely inspect the previous assumptions and results by more extensive numerical calculations. Table I summarizes our main results. In several cases, the correlation functions flip their signs around the middle of the chain (see Sec. III A). This allows us to define an order parameter with reversed sign in the thermodynamic limit. We also find that in some of the cases with sign-flipping order parameter superfluid correlations show a quasialgebraic behavior (see Sec. III C).

III. CORRELATION FUNCTIONS

In this section we investigate string, density, parity, and superfluid correlations in the ground states of the MI, HI, and DW phases. To this end, we carry out MPS based DMRG calculations with site occupations truncated at $n_{\max} = 4$ and a maximum bond dimension of $\chi_{\max} = 250$ [12], which is sufficient for numerical convergence. Throughout the paper,

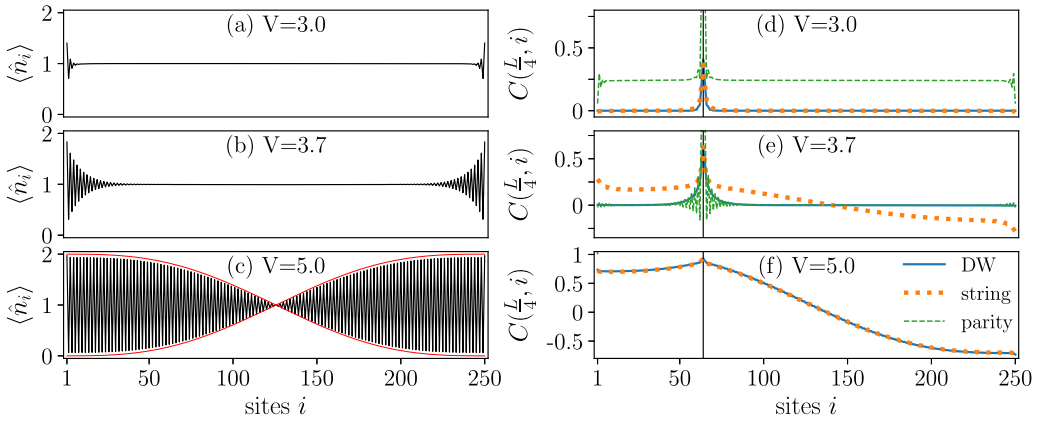

FIG. 2. Boundary condition (A) for $L = 250$, $U = 6$ and from top to bottom $V = 3.0$ (MI), 3.7 (HI), 5.0 (DW). The left panels (a)–(c) depict occupation patterns. In (c) the red line represents the envelope calculated from the domain-wall states in Eq. (8). The right panels (d)–(f) show string (dotted orange), DW (solid blue), and parity (dashed green) correlation functions $C(L/4, i)$. Vertical lines indicate the maxima at $L/4$. Rapidly oscillating C_{par} is omitted in panel (f).

we assume a large on-site interaction $U = 6$, and most of the results are for up to $L = 250$ sites.

We first discuss the dependence of the three correlation functions, C_{DW}, C_{parity}, and C_{str}, and of the site occupation on the boundary conditions. Second, we show the dependence of the corresponding order parameters on V. Finally, we study the SF correlation functions.

A. String, density, and parity correlations

1. Case (A)

Let us first consider boundary condition (A). Figures 2 and 3 show the site occupations and correlation functions for $L = 250$ (A even) and $L = 251$ (A odd), respectively. The left panels show the site occupations of selected ground states. In the DW phase of the even chain [see Fig. 2(c)], there is a change from an up-down to a down-up pattern in the middle of the chain. We checked that this pattern scales with the size of the system, which is why we call it a macroscopic boundary effect. In contrast, such a pattern does not appear in the odd case [see Fig. 3(c)]. The oscillations found at the edges in the MI and HI phases [see Figs. 2(a) and 2(b)] do not scale with the system size.

In the right panels of Figs. 2 and 3, we depict the corresponding string, density, and parity correlation functions evaluated between site $\approx L/4$ and all other sites i:

$$C(L/4, i). \tag{7}$$

One can clearly distinguish MI, HI, and DW, depending on which correlations decay to zero; a more detailed discussion will be given in Sec. III B. We find that some of the correlation functions remain nonzero, while they flip signs in the middle of the chain. These sign flips are stable under finite-size scaling. In the case of (A even), the string correlation changes its sign in the HI phase, and both string and density correlations flip their signs in the DW phase [Figs. 2(e) and 2(f)]. On the other hand, in the case (A odd) only the string correlation behaves in this way in the HI and DW phases [Figs. 3(e) and 3(f)]. The absence of a sign flip of the density correlation function of the odd chain is consistent with the uniform occupation pattern in Fig. 3(c).

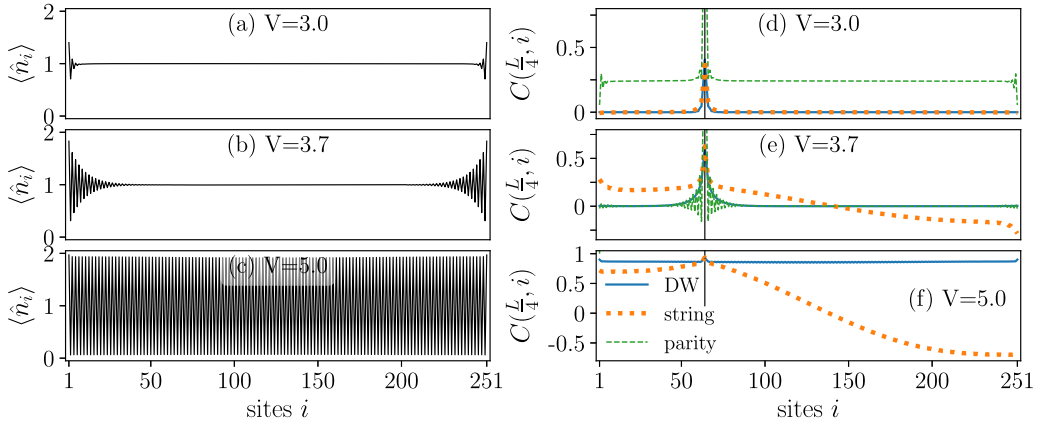

FIG. 3. Boundary condition (A) for $L = 251$, $U = 6$ and from top to bottom $V = 3.0$ (MI), 3.7 (HI), 5.0 (DW). The left panels (a)–(c) depict occupation patterns; the right panels (d)–(f) show string (dotted orange), DW (solid blue), and parity (dashed green) correlation functions $C(L/4, i)$. Vertical lines indicate the maxima at $L/4$. Rapidly oscillating C_{par} is omitted in panel (f).

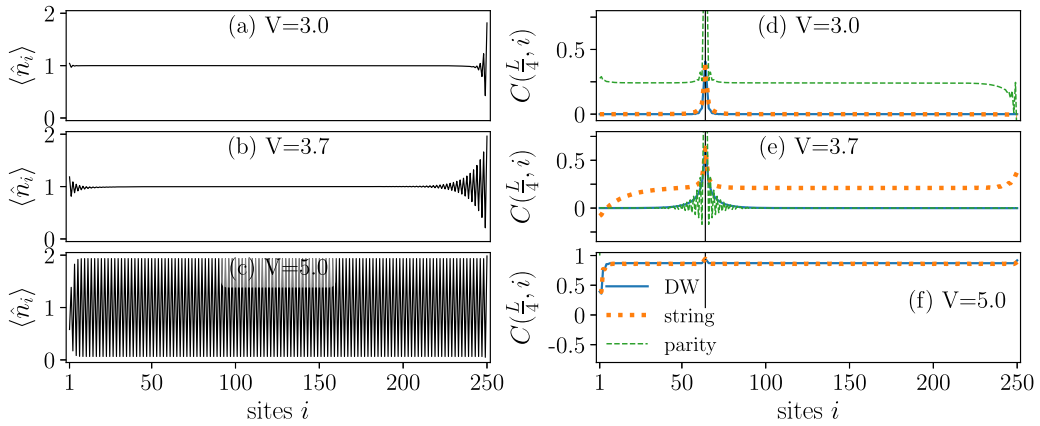

FIG. 4. Boundary condition (B) for $L = 250$, $U = 6$ and from top to bottom $V = 3.0$ (MI), 3.7 (HI), 5.0 (DW). The left panels (a)–(c) depict occupation patterns; the right panels (d)–(f) show string (dotted orange), DW (solid blue), and parity (dashed green) correlation functions $C(L/4, i)$. Vertical lines indicate the maxima at $L/4$. Rapidly oscillating C_{par} is omitted in panel (f).

The DW patterns can be understood by the fact that both edge populations are pinned to $\langle \hat{n}_{1,L} \rangle \approx 2$, which creates a domain wall in between. The edge populations are pinned because of the lack of one nearest neighbor at the edge. In the spin model, this is encoded by the effective edge fields in Eq. (6). Assuming a simple effective picture in the limit $V \gg U \gg J$, the dominant configurations for (A even/odd) have a domain wall as

$$|\psi_j\rangle = \begin{cases} |20\ldots2020\rangle\,|0202\ldots02\rangle & \text{(A even)}, \\ |20\ldots2020\rangle\,|1\rangle\,|0202\ldots02\rangle & \text{(A odd)}, \end{cases} \tag{8}$$

where the domain wall is located at site $\approx 2j$ [see also Fig. 1(b), cases $\text{DW}^{\star}_{\text{even/odd}}$]. From this, it is clear that the staggered density modulations change signs only in the even case. As is shown in Appendix A, the ground state approximately takes the following form:

$$|G\rangle = \sum_j w_j\,|\psi_j\rangle \sim \sum_j \sin\left(\frac{\pi\, j}{d+1}\right)|\psi_j\rangle\,, \tag{9}$$

where d is the number of domain-wall states, $|\psi_j\rangle$ is a domain-wall state such as Eq. (8), and $j = 1, \ldots, d$ are labels of possible positions of the domain wall. This leads to the envelope indicated in Fig. 2(c) (see the red line).

In contrast to the density correlation function, the string correlation function is not sensitive to even and odd distances. In the DW phase, the domain-wall configurations in Eq. (8) both give spin-flipping string correlations. We can interpret the sign flip of C_{str} in the HI phase along the same lines. Because with boundary condition (A) doublons prefer to locate near the edges, a domain-wall-like structure is created in between [see Fig. 1(b), case $\text{HI}^{\star}$, for an illustration]. This occurs regardless of whether L is even or odd, and it is consistent with a sign flip of string correlations. A toy wave function that captures this sign flip of string correlations is given by [8]

$$|\psi_j\rangle = \hat{a}_1^{\dagger} \prod_{i=1}^{j-1} (\hat{a}_i^{\dagger} + \hat{a}_{i+1}^{\dagger}) \prod_{i=j+1}^{L-1} (\hat{a}_i^{\dagger} + \hat{a}_{i+1}^{\dagger}) \hat{a}_L^{\dagger}\,|0\rangle\,. \tag{10}$$

The expectation value of a local density fluctuation $\langle \delta n_i \rangle$ of this state adds up to $\approx 1/2$ near the edges (i.e., edge states), and to $\approx -1/2$ near the sites j and $j+1$ corresponding to a domain wall. In Appendix A 1 we argue that the same ansatz as for the DW phase, i.e., $|G\rangle \sim \sum_{j=1}^{L-1} w_j\,|\psi_j\rangle\,/\sqrt{\langle\psi_j|\psi_j\rangle}$ with weights w_j given in Eq. (9), qualitatively describes the ground state in the HI phase. Quantitative deviations from the precise DMRG calculations are mainly due to neglected fluctuations in the toy states $|\psi_j\rangle$ in Eq (10). As will be discussed in Secs. III C and IV, this ansatz also leads to SF correlations and an entanglement entropy that qualitatively agrees with the DMRG results.

2. *Case (B)*

Let us now turn to boundary condition (B), which is depicted in Fig. 4. Note that we restrict the present discussion to the even system size L, as there is no significant difference to the odd case (see Appendix B). We see that the left edge potential, $\mu > 0$, favors an empty state, while the right edge potential, $-\mu < 0$, favors a doubly occupied state, and the inversion symmetry is broken. Therefore, the occupation pattern in the DW phase [Fig. 4(c)] as well as string and density correlations [Figs. 4(e) and 4(f)] show a uniform bulk behavior. The edge potentials of (B) have eliminated the macroscopic boundary effects of case (A), i.e., the macroscopic envelope of the occupation pattern and sign flips of the correlation functions. This is also seen in the entanglement entropies in Sec. IV and in the entanglement spectra in Appendix E.

The results can be understood as follows. For (A), which corresponds to (B) with $\mu = 0$, the domain walls of the HI and DW phases are located in the center of the system. By adiabatically increasing μ, one observes that the domain walls migrate from the center to one of the edges of the chain. Qualitatively, the weights of the effective ground state start as in Eq. (9) for $\mu = 0$ and then change, such that eventually the weight of $|02\ldots02\rangle$ dominates. As we show in Appendix A 2, sufficiently far away from the HI-DW transition, the ground state is part of a low-energy band spanned by the states $|\psi_j\rangle$ in Eq. (8). The band consists of the domain walls

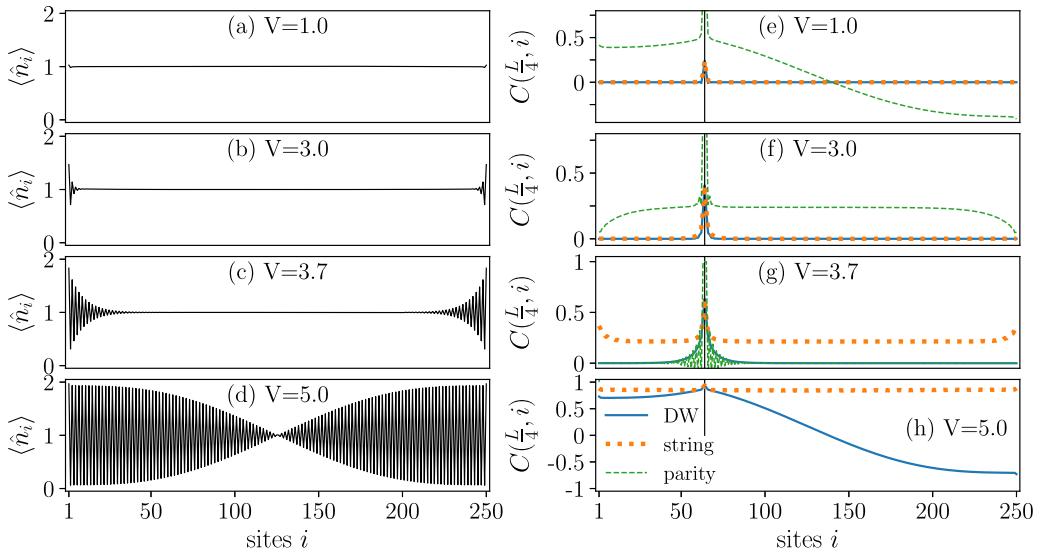

FIG. 5. Boundary condition (C) for $L = 250$, $U = 6$ and from top to bottom $V = 1.0, 3.0$ (MI), 3.7 (HI), 5.0 (DW). The left panels (a)–(d) depict occupation patterns; the right panels (e)–(h) show string (dotted orange), DW (solid blue), and parity (dashed green) correlation functions $C(L/4, i)$. Vertical lines indicate the maxima at $L/4$. Rapidly oscillating C_{par} is omitted in panel (h).

with effective tunneling amplitude $\tilde{J} \sim J^2/(V - U)$ for $V \gg U \gg J$. The value of μ necessary to remove the domain wall is on the order of the corresponding bandwidth $\approx \tilde{J}$. We can therefore interpret the transition from (A) to (B) in terms of a competition between the effective kinetic energy of the domain wall and the localizing edge potentials. In the limit $V \to \infty$, the bandwidth vanishes and the basis states of Eq. (8) are degenerate ground states, such that an infinitesimal μ is sufficient to remove the sign flips. On the other hand, in the present case of $V = 5$ and $U = 6$, a large value of $\mu = 2J$ is necessary. While the effective picture breaks down for these parameters, we checked by exact diagonalization that the bandwidth is $\approx 1.5J$ (see Appendix A 2).

3. Case (C)

For condition (C), we have one extra boson, i.e., $N = L + 1$. This extra boson has indeed restored a uniform string correlation in the HI and DW phase [Figs. 5(g) and 5(h)]. However, for L even the density correlation function and the occupation pattern [Figs. 5(d) and 5(h)] in the DW phase show the same sign flip as for (A even). This can again be illustrated in terms of a domain-wall state. In the present case (C even), the additional particle is placed on the domain-wall state of (A even), which can be effectively expressed by patterns such as

$$|20\ldots203020\ldots20\rangle\,|0202\ldots02\rangle\,. \tag{11}$$

For these states, the sign flip disappears for C_{str}, but persists for C_{DW}. In Sec. IV we argue based on the spatial dependence of the entanglement entropies that the extra boson is bound to the domain wall, and hence the relevant domain-wall states in this case look like

$$|\psi_j\rangle = |20\ldots20\underline{3}0\rangle\,|0202\ldots02\rangle\,. \tag{12}$$

We note that the case (C odd) gives a trivial density wave without domain wall, well described by the state

$$|20\ldots20202\ldots02\rangle\,. \tag{13}$$

This is numerically confirmed in Appendix B.

One difference of condition (C) compared to (A) and (B) appears in the small V regime, $V \lesssim 3.5$. For the boundary conditions (A) and (B), this regime corresponds to the MI phase. In case (C), instead, we find two distinct regimes of nonzero parity order: (i) for $V \lesssim 2.4$ the parity correlation function flips sign [see Fig. 5(e)] and (ii) for $2.4 \lesssim V \lesssim 3.5$ it settles to a constant value [see Fig. 5(f)]. The reason for this, as we show explicitly in Sec. III D, is that the extra boson localizes at the edges when V is increased. Therefore, in the regime (ii) with higher V, the bulk is effectively undoped. From the perspective of the doping, we then expect the lower V regime to have nonzero SF correlations and the larger V regime to be a pure MI, which we examine more carefully in Sec. III C. However, the present results show that the state in the low V regime must be distinct from a pure bulk SF state, because parity correlations decay to zero in the pure SF phase. We interpret it as a MI with additional off-diagonal long-range correlations induced by states such as

$$|\psi_j\rangle = |1\ldots1\rangle\,|2\rangle\,|1\ldots1\rangle\,, \tag{14}$$

which hosts an additional single particle at site j. Sufficiently far from the additional particle, fluctuations are still predominantly doublon-holon pairs [see Fig. 1(b), case MI*].

B. Order parameters

Here we discuss the order parameters, O_{DW}, O_{parity}, and O_{str}. In practice, due to the finite size of the system, we choose $O = C(L/4, 3L/4)$. Since this definition involves fixed sites relative to the system size, we can obtain well-defined values even for the sign-flipping cases.

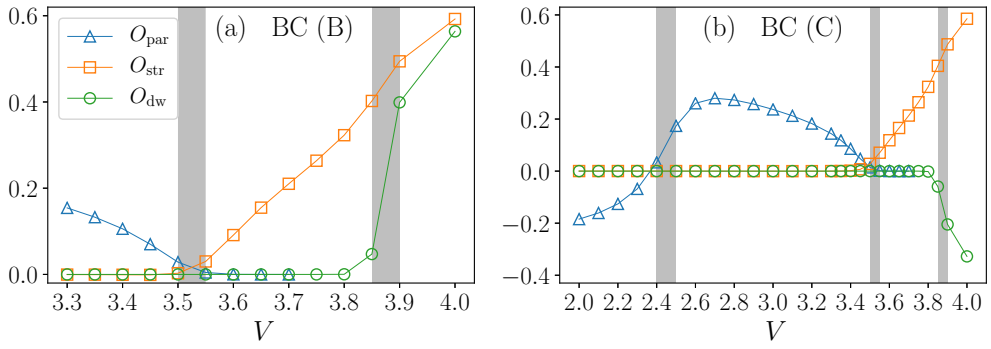

FIG. 6. Order parameters $O_{\rm par}$, $O_{\rm str}$, and $O_{\rm DW}$ as a function of V for $U = 6$ and $L = 250$ with boundary condition (B) in panel (a) and boundary condition (C) in panel (b). Shaded areas indicate the position of critical points as narrowed down by a finite-size analysis.

First, we find that the positions of critical points do not significantly depend on the boundary condition. In Fig. 6, we show the order parameters as functions of V for case (B), where edge potentials support well-defined bulk phases, and for case (C), where an extra particle, $N = L + 1$, is added. In both cases, our finite-size analysis narrowed down the MI-HI transition to $V^c_{\text{MI-HI}} \approx 3.525 \pm 0.025$ and the HI-DW transition to $V^c_{\text{HI-DW}} \approx 3.875 \pm 0.025$. For case (A even/odd), the phase boundaries fall into the same range (not shown). The robustness of the phase boundaries to different boundary conditions is due to the fact that the influence of a domain wall on the local properties of the state vanishes in the thermodynamic limit. The negative value of $O_{\rm DW}$ in case (C) is due to the sign flip of $C_{\rm DW}$.

Second, in Fig. 6(b) for case (C), one can see an extra transition from a sign-flipping to a constant parity correlation function around $V \approx 2.4$, which does not exist for boundary conditions (A) and (B). As is shown below, this additional transition is accompanied by a transition from algebraic to exponential decay of SF correlations, which is caused by the localization of the extra particle to the edge sites due to strong V.

C. Superfluid order

Let us now take a look at the spatial dependence of superfluid correlations. To this end we compare the boundary conditions (A), (B), and (C) in Fig. 7. For each case, we plot $C_{\rm SF}(L/4, L/4 + r)$ with $L = 250$ for four selected ground states far from criticality and one ground state close to the MI-HI transition. For boundary condition (A) and $V = 5$, representing the DW phase, we have included the case of an odd chain, $L = 251$, because it differs from the even chain.

In all three cases, $C_{\rm SF}$ decays by power law near the MI-HI transition (yellow lines). This is in agreement with Ref. [8], where it was shown that at this transition the system behaves as a Tomanaga-Luttinger liquid. On the other hand, $C_{\rm SF}$ decays exponentially in the MI phase (light blue lines, $V = 3.0$) regardless of the boundary conditions. With boundary condition (C), $C_{\rm SF}$ goes up again at large distances due to the extra particle localized close to the edges. With $V = 1$ (purple lines), the boundary conditions (A) and (B) again give a MI phase and $C_{\rm SF}$ decays exponentially. By contrast, the boundary condition (C) leads to a power-law decay of $C_{\rm SF}$ at short distances, followed by a plateau. Here the extra particle is delocalized over the whole chain, as indicated by the sign

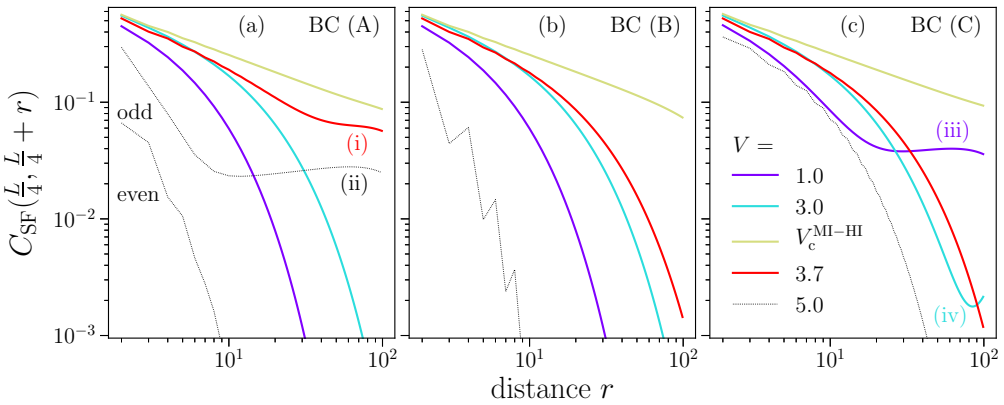

FIG. 7. SF correlation functions $C_{\rm SF}(L/4, L/4 + r)$ for $L = 250$ with boundary conditions (A), (B), and (C). The values of V are chosen as $V = 1.0$ [MI for (A) and (B), SF for (C)], $V = 3.0$ (MI), $V_c^{\text{MI-HI}} = 3.5$ for (A) and (B) and 3.55 for (C) (closest to critical power law), and $V = 3.7$ (HI). For the case of odd $L = 251$ in the DW phase in panel (a), we only show values for even r due to strong oscillations of $C_{\rm SF}$. The colored labels (i)–(iv) mark the graphs that show significant boundary effects in the order that they are discussed in the text and shown in Fig. 8.

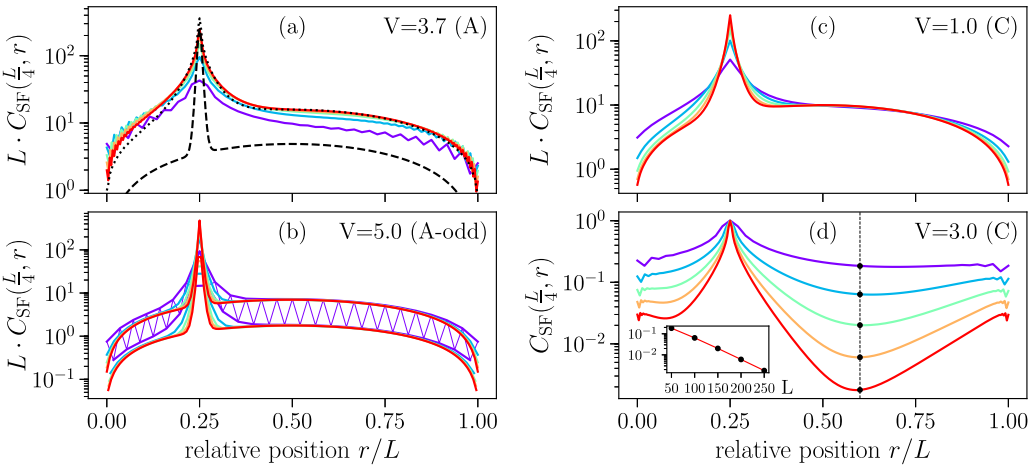

FIG. 8. Finite-size scaling of SF correlation functions [from $L = 50$ (purple) to 250 (red)] for the four cases of Fig. 7, which are neither power law nor exponential. The relative distance r/L corresponds to r_2 in Eqs. (15)–(17). In panels (a), (b), and (c) we have rescaled C_{SF} by the factor L. The dotted plot in (a) shows a DMRG calculation of the spin-1 model (5) with edge fields (6) for $U = 5$, $V = 3.4$ (Haldane phase), where $\langle \hat{a}_i^\dagger \hat{a}_j \rangle$ has been replaced by $\langle \hat{S}_i^+ \hat{S}_j^- \rangle$; the dashed line in (a) comes from a simple domain-wall picture for the HI phase. In case (b) the correlations at even and odd distances are plotted separately and oscillations are shown for $L = 50$. The inset of panel (d) indicates exponential decay of $C_{\mathrm{SF}}(0.25L, 0.6L)$ as a function of L.

flip of the parity correlation function in the previous section. In the HI phase (red lines, $V = 3.7$), the SF correlations decay exponentially with boundary conditions (B) and (C). However, with boundary condition (A) in the sign-flipping HI phase, the correlations are enhanced. Here we see a power-law decay followed by a plateau at larger distances. Finally, in the DW phase with $V = 5$ (grey lines) we see exponential decay of C_{SF} for (A even), (B), and (C), whereas (A odd) gives a power law followed by a plateau.

We further investigate the system size dependence of the four cases where C_{SF} decays neither exponentially nor purely in a power-law manner (see labels in Fig. 7): (i) $V = 3.7$ with BC (A), (ii) $V = 5.0$ with BC (A odd), (iii) $V = 1$ with BC (C), and (iv) $V = 3.0$ with BC (C). In the first three cases, (i)–(iii), the influence of the edge appears as a macroscopic plateau, and we plot C_{SF} rescaled by the factor L in Figs. 8(a)–8(c):

$$\tilde{C}_{\mathrm{SF}}(r_1, r_2; L) \equiv L C_{\mathrm{SF}}(r_1 L, r_2 L), \tag{15}$$

where $r_{1,2} \in [0, 1]$ denotes the relative position in the chain. The convergence of the curves indicates that, as $L \to \infty$, the plateaus scale as

$$C_{\mathrm{SF}}(r_1 L, r_2 L) \sim L^{-1}. \tag{16}$$

Therefore, we conclude that these states show quasi-long-range superfluid correlations. The similarity among (i), (ii), and (iii) suggests that in all three cases a single-particle-like excitation is responsible for the quasi-long-range order.

On the other hand, for case (iv) [Fig. 8(d)], we find that as a function of L

$$C_{\mathrm{SF}}(r_1 L, r_2 L) \sim e^{-L\gamma(r_1, r_2)} \tag{17}$$

for $r_1 = 0.25$ and any $r_2 \in [0, 1]$. For roughly $r_2 \in [0.3, 0.5]$ the factor in the exponent behaves as $\gamma(r_1, r_2) \sim |r_1 - r_2|$, which corresponds to an undoped MI. If we plotted $C_{\mathrm{SF,L}}$ in this range for various L's in absolute distance scales, they would lie on top of each other. On the other hand, when $r_2 \gtrsim 0.6$, the correlations increase again, due to the extra particle. However, the value at the edge, $\tilde{C}_{\mathrm{SF}}(0.25, 1; L)$, still decays exponentially as the system size L increases, and hence we conclude that there is no superfluid order in this case.

For case (i), the picture of a single defect is further supported by a DMRG calculation of the spin-1 model from Eq. (5) with edge fields as in Eq. (6), which shows a very similar behavior [see the dotted black line in Fig. 8(a)]. By analogy, C_{SF} is replaced by $\langle \hat{S}_i^+ \hat{S}_j^- \rangle$. To a good approximation this model amounts to setting a cutoff at $n_{\max} = 2$. Therefore, large local particle number fluctuations $n > 2$ are irrelevant here, in contrast to a bulk superfluid.

Moreover, we can compare our DMRG results on C_{SF} in case (i) with an analytical estimate given by the domain-wall wave function in Eq. (9) with basis states $|\psi_j\rangle$ from Eq. (10) [dashed black line in Fig. 8(a), calculated according to Appendix C]. In this ansatz, site occupations are restricted to $n \leqslant 2$ as in the spin-1 model. We find a qualitatively similar correlation function as the numerically exact one calculated by DMRG. However, with the toy wave function, C_{SF} decays much faster at short distances and the value of the plateau is almost an order of magnitude lower. In Appendix C we show that the plateau value can essentially be understood in terms of the overlaps of domain-wall states $\langle \psi_i | \psi_j \rangle / \sqrt{\langle \psi_i | \psi_i \rangle} \sqrt{\langle \psi_j | \psi_j \rangle}$. These overlaps decay approximately exponentially with decay length $[\ln(1 + \sqrt{2})]^{-1} \approx 1.3$ in units of the lattice constant; by artificially setting a larger decay length ≈ 4, i.e., assuming wider domain walls, the height of the plateau can be reproduced, while the weights in Eq. (9) determine only the shape of the plateau. Thus, the toy states underestimate the true width of the domain walls.

D. Edge occupations

One of the main arguments of the previous sections is based on an increased particle density close to the edges and hence a doping of the bulk. To confirm this interpretation, in

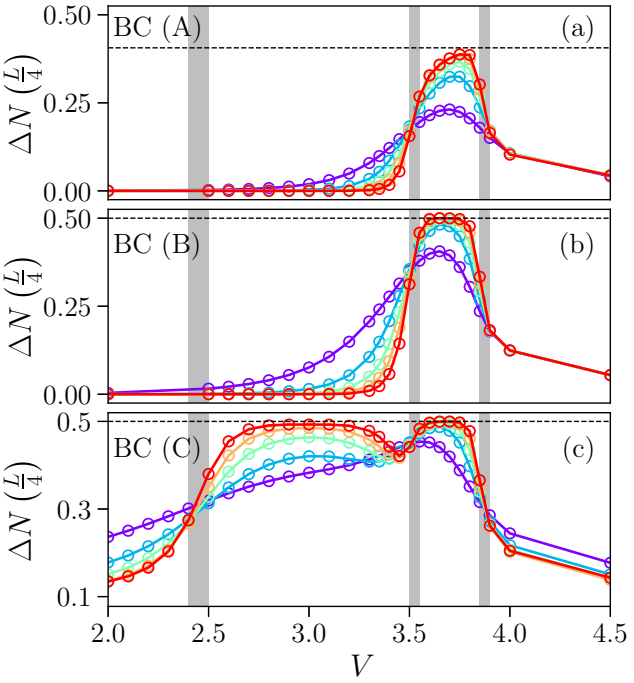

FIG. 9. Excess densities ΔN of the quarter of the chain close to the right edge as a function of V for system sizes from $L = 50$ to 250. Reading from top to bottom, the boundary conditions (A), (B), and (C) were used. In panel (a) the dashed black line indicates the value due of ΔN for a domain-wall state as in Eq. (10) with a sinelike wave function. Panel (b) shows occupation numbers from the edge with negative potential.

Fig. 9 we plot the excess population

$$\Delta N(l) = \left(\sum_{i=1}^{l} \langle \hat{n}_i \rangle - 1\right) \tag{18}$$

of the first $l = L/4$ sites as a function of V for system sizes from $L = 50$ to 250.

For boundary condition (A) we do not see a quantization of ΔN to 1/2 [Fig. 9(a)]. However, increased edge population in the HI phase, $3.5 \lesssim V \lesssim 3.9$, is consistent with the value given by the toy states in Eq. (10) [dashed black line in panel (a), see Appendix C]. Note that in Fig. 8(a) the case $i = L/4$ is shown and agrees well with DMRG. This is not surprising, as both the toy states and the DMRG results have $\langle n_i \rangle = 1$ in the bulk. On the other hand, the edge potentials of boundary condition (B) and the extra boson of (C) lead to 1/2-edge states in the HI phase [Figs. 9(b) and 9(c)]. In addition, in case (C), one clearly sees that for $2.4 \lesssim V \lesssim 3.5$ the extra particle localizes at the edges. This confirms our interpretation of the correlation functions and the plateau of the entanglement entropy as representing a MI phase.

IV. ENTANGLEMENT ENTROPY

In Sec. III we found that certain boundary conditions induce quasi-long-range SF order in parameter regimes which typically belong to the MI, HI, or DW phase, where correlation functions of the original insulating phases flip merely their signs. In order to check whether the quasi-long-range SF correlations indeed imply the critical properties of a bulk SF phase or are merely an artifact of a single defect, we now investigate the entanglement entropies. If the system is truly in a bulk SF phase, as mentioned in Sec II A, the block entropies $S_L(l)$ are marked by a characteristic dependence on the position l of the bipartition [see Eq. (4)] as well as a logarithmic divergence in the system size L (volume law). On the other hand, if the SF correlations come from a domain wall, we expect a finite contribution to the entropy that does not diverge as L increases.

In Fig. 10, we plot the block and system size dependence of the entanglement entropies, focusing on the same representative cases $V = 1.0, 3.0, 3.7, 5.0$ as in Sec. III. In every case, we see a saturated plateau of $S_L(l)$ that does not depend on L for boundary condition (B). This agrees with the absence of quasi-long-range SF correlations. If there is a single domain wall on top of a regular bulk background, we expect that the entanglement entropy can be written as a sum of two contributions. In order to calculate the contribution from the domain walls, let us consider a state $|G\rangle$ given by the superposition of local domain-wall wave functions $|\psi_j\rangle$ e.g., given in Eqs. (8), (10), (12), and (14). We assume that the weight of each $|\psi_j\rangle$ is given by Eq. (9), i.e.,

$$\begin{aligned} |G\rangle &= \sum_{j=1}^{d} w_j \, |\psi_j\rangle \\ &= \sum_{j<m_l} \sin\left(\frac{\pi j}{d+1}\right) |\psi_j\rangle + \sum_{i \geqslant m_l} \sin\left(\frac{\pi j}{d+1}\right) |\psi_j\rangle \,, \end{aligned} \tag{19}$$

where the two terms correspond to the domain-wall states the centers of which are left or right of the bipartition point between sites l and $l+1$, and m_l is the smallest index of the domain wall in the right block. The two contributions in Eq. (19) can have an overlap due to configurations where the domain wall is close to site l, either on the left or the right, due to a finite width of the domain wall ($\langle \psi_{j'} | \psi_j \rangle \neq 0$, see discussion below). However, in the thermodynamic limit the local influence of the domain wall at site l vanishes. Hence, we ignore the overlap of the two contributions. In this limit, as we show in Appendix D, the entropy from the domain-wall state $S_L^{\text{extra}}(l)$ simplifies to

$$S_L^{\text{extra}}(l) \xrightarrow[l/L=\text{const.}]{L\to\infty} -p_l \ln(p_l) - (1-p_l)\ln(1-p_l), \tag{20}$$

with

$$p_l = \frac{\sum_{i \leqslant m_l} \sin^2\left(\frac{\pi i}{d+1}\right)}{\sum_{i \leqslant d} \sin^2\left(\frac{\pi i}{d+1}\right)}. \tag{21}$$

We note that the result is equivalent to the entanglement entropy for the ground state of a tight-binding model with a single particle in an open chain. This naturally explains the similarly of the results for the domain walls and the extra particle.

For comparison with DMRG, we add the plateau value from boundary condition (B) to the domain-wall contribution

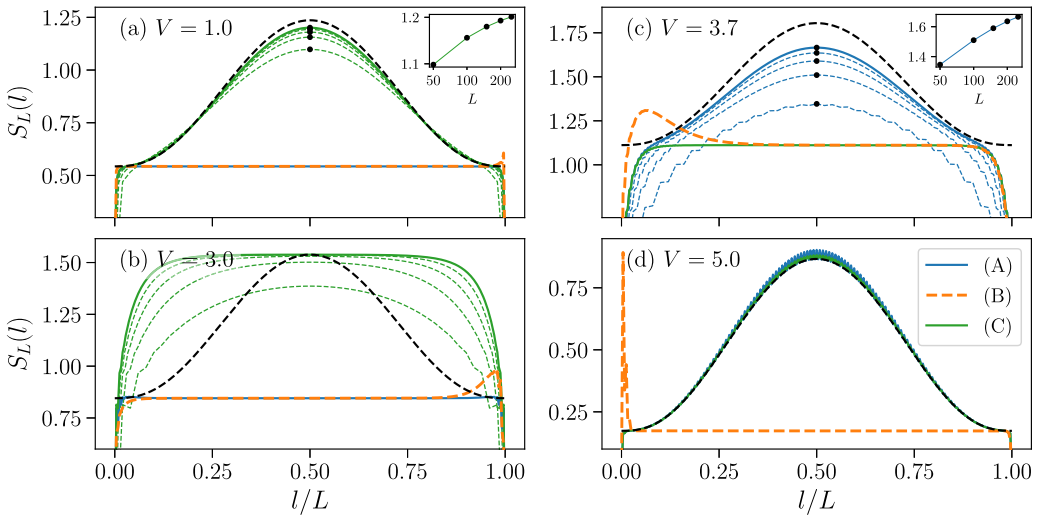

FIG. 10. Block entropies of the left block as a function of block size over system size l/L for $L = 250$. Boundary conditions (A) [blue lines], (B) [green lines], and (C) [dashed orange lines] are compared for $V = 1.0, 3.0, 3.7, 5.0$ [panels (a), (b), (c), and (d), respectively]. Dashed black lines are the values calculated from the effective theory (see Appendix A 1) added onto the plateau value of boundary condition (B). Thin dashed lines in (a), (b), and (c) represent system sizes $L = 50, 100, 150, 200$ for (C) and (A), respectively. The insets show the values marked by black dots in the main figures, plotted against the logarithmic system size.

in Eq. (20), and plot the result in Fig. 10 (dashed black lines).[1] This is different from the result of a conformal field theory [see Eq. (4)], which excludes the possible gapless phase that was anticipated in Ref. [23].

In the low V regime, $V \lesssim 3.5$ [see Figs. 10(a) and 10(b)], boundary condition (A) gives the same plateau as (B). With boundary condition (C), the entropy $S_L(L/2)$ of the symmetric bipartition saturates at $\approx \ln 2$ above this plateau; the inset of panel (a) shows that $S_L(L/2)$ does not diverge logarithmically. For $V = 1$ the dependence on the bipartition converges to the prediction of the sine-like wave function [see panel (a)]. Therefore, the extra boson is approximately described by this wave function. Meanwhile, for $V = 3$, we have a broad plateau, which is due to the localization of the extra boson at the edges [see panel (b)]. In both cases, finite-size effects can be understood by additional number fluctuations, which are due to the extra boson. These cause finite overlaps of the effective basis states in Eq. (19).

In the HI regime, $3.5 \lesssim V \lesssim 3.9$, boundary condition (C) agrees with the bulk value [see Fig. 10(c)]. Here, the entropies for boundary condition (A) approach the domain-wall prediction, and $S_L(L/2)$ increases slower than logarithmically [see the inset of panel (c)]. However, the convergence is much slower than in the single-particle case of panel (a). The slow convergence of the entropies points to a large overlap of the contributions of Eq. (19). This overlap can be qualitatively understood in terms of Fig. 1(b), case HI*. Namely, the domain wall can lie anywhere between the two occupations of $n = 0$ that are highlighted in the figure, which indicates a larger width of the domain wall.

As for the DW phase, $V = 5.0$, we see the domain-wall picture very well confirmed by the DMRG simulations for both boundary condition (A) and (C) [see Fig. 10(d)]. We recall the low-energy effective states of boundary condition (C) [see Eq. (11)], where the extra boson is added to the effective states of boundary condition (A) [see Eq. (8)]. Naively, one might expect that this further increases the entropy up to an additional factor of $\approx \ln 4$ instead of $\approx \ln 2$ above the bulk value, because both the extra boson and the domain wall can either be on the left or on the right. The fact that the entropy is only increased by $\approx \ln 2$ can be understood by the extra boson being bound to the domain wall. Let us consider the configurations of Eq. (12), where the extra boson is next to the domain wall. These are energetically favored, because virtual configurations $\ldots 2021|0202 \ldots$ (next to the domain wall) are favored compared to $\ldots 202120 \ldots$ (away from the domain wall) due to the nearest-neighbor interaction.

Altogether we conclude that in all cases a single-particle-like defect is responsible for enhanced SF correlations. Since the entanglement entropies do not diverge with the system size, these do not indicate a bulk SF phase. However, it is well known that superfluid order emerges if we fix a nonzero doping density instead of doping with a single particle as in case (C) (see, e.g., Ref. [16]). In that case, we do not expect that macroscopic boundary effects exist as in the present paper, because infinitely many defects appear in the thermodynamic limit.

V. CONCLUSION

In this paper we have investigated the influence of various open boundary conditions on the ground states of the 1D extended Bose-Hubbard model at or near unit filling. We have found that the simple open chain at exactly unit filling has a nondegenerate ground state, even in the Haldane insulator and density wave regimes. In particular this means that the Haldane insulator does not have two degenerate edge state configurations, as would be naively expected. This can be

[1] In the DW phase we have not accounted for site-to-site oscillations of the probabilities p_l.

explained by the fact that the nearest-neighbor interaction V effectively induces attractive edge potentials, causing a higher population of the edges and the presence of a domain wall around the middle of the chain. If the system is doped with a single extra boson, the regime corresponding to the Mott insulator splits in two regimes, where the extra boson behaves like the domain walls for low V and is trapped at the edges for larger V.

In most cases the domain wall induces algebraic behavior of the off diagonals of the single-particle density matrix. However, this is not an indication of a fundamental change of the bulk order, but an artifact of the domain wall. Interestingly, in the density wave regime with even L, the domain wall has a different character, which leads to a modulation of the density wave pattern on the scale of L, but not to quasi-long-range order.

Our results demonstrate that boundary conditions can have a significant influence on quantum many-body states, if interactions beyond contact interaction are present. Local potentials at the edges may be used to control the effective filling factor. On the other hand, such effects can be a hindrance to the physical control of topological edge states, as these can be naturally pinned to one value.

ACKNOWLEDGMENTS

The authors thank M. Thoss for helpful comments on the paper. We acknowledge support by the state of Baden-Württemberg through bwHPC and the German Research Foundation (Deutsche Forschungsgemeinschaft) through Grant No. INST 40/467-1 FUGG. J.O. acknowledges support from Research Foundation for Opto-Science and Technology and from Georg H. Endress Foundation.

APPENDIX A: DOMAIN-WALL STATES

1. General discussion

Here we give a heuristic discussion of the domain-wall ground states referred to in Secs. III and IV. As above, let $j = 1, \ldots, d$ denote labels for possible positions of the domain wall along the chain, ordered from left to right, and let $|\psi_j\rangle$ denote the corresponding states. We assume that the ground state is well captured within this reduced Hilbert space of domain-wall states. In certain limiting cases outlined below, this description is indeed exact. Furthermore, the numerical results of sign-flipping correlation functions, algebraic SF correlations, and entanglement entropies indicate that this picture is qualitatively correct even in intermediate parameter regimes. However, one may have to assume that in these regimes the domain wall has a finite width and, therefore, the basis states are not orthogonal [see the discussion below Eq. (20) in Sec. IV].

An effective Hamiltonian $\hat{H}_{\text{eff}}$ acting on the domain-wall states consists, to zeroth order, of the projection of the full Hamiltonian $\hat{H}$ onto those states. Higher-order contributions involve multiple hoppings via virtual states, and, in general, there will be arbitrarily far off-diagonal terms in the effective Hamiltonian. These couplings decay more slowly when the domain wall has a broader width. However, the technicalities of nonorthogonal basis sets do not affect our argument and are, therefore, not discussed (see, e.g., Ref. [31]). Rather, we start from the following form of $\hat{H}_{\text{eff}}$ assuming that the matrix elements $(\hat{H}_{\text{eff}})_{ij}$ depend only on the distance of the two domain walls involved, i.e.,

$$\hat{H}_{\text{eff}} = \begin{pmatrix} D & J_1 & J_2 & \cdots & J_{d-1} \\ J_1 & D & \ddots & \ddots & \vdots \\ J_2 & \ddots & \ddots & & J_2 \\ \vdots & \ddots & & D & J_1 \\ J_{d-1} & \cdots & J_2 & J_1 & D \end{pmatrix}. \tag{A1}$$

The explicit form of the matrix elements can be calculated by perturbation theory. Deviations are only expected for i, j near the edges in comparison to the width of the domain wall. This is equivalent to a single particle on a chain where the hopping amplitude between two sites separated by r sites is given by J_r and the onsite energy is given by D. The eigenstates $|k\rangle$ of any Hamiltonian of the form of Eq. (A1) are given by [32]

$$|k\rangle \propto \sum_j \sin\left(\frac{\pi jk}{d+1}\right)|\psi_j\rangle\,, k = 1, \ldots, d, \tag{A2}$$

where the corresponding energies are

$$E_k = D + 2\sum_r J_r \cos\left(\frac{\pi rk}{d+1}\right). \tag{A3}$$

For a short-ranged Hamiltonian with $J_1 < 0$, $k = 1$ corresponds to the ground state, which motivates our assumption of the sine-like wave function of the domain wall of Eq. (9). The agreement of this ansatz with our numerical results on the spatial behavior of the entanglement entropies in Fig. 10 suggests that the ground state corresponding to the $(k = 1)$ mode is indeed a good description.

On the other hand, excited states of the effective Hamiltonian are given by modes with higher k. Within the reduced Hilbert space, this picture needs to be modified for wave lengths on the order of the width of the domain wall, because the wave function has significant weights on states where Eq. (A1) does not hold. Moreover, the reduced Hilbert space itself might not be sufficient, if excitation energies in the effective model are on the order of the bulk excitation gap.

The energy spectrum is gapless, due to long-wave-length modes of the domain wall. Even though this can lead to algebraic behavior of the off diagonals of the single-particle density matrix, gapplessness does not imply a bulk superfluid phase. The reason is that the low-energy excitations are not bulk properties, but properties of a single defect, i.e., the domain wall. In other words, the off-diagonal long-range order can be understood in terms of $O(L)$ domain-wall states, without requiring exponentially many occupation number basis states.

An example for basis states with domain walls of width zero is given in Eq. (8). It describes the ground state of the DW phase with boundary condition (A even) in the limit $V \gg U \gg J$ with effective Hilbert-space dimension $d = L/2 + 1$. The assumption of a zero width domain wall is motivated for intermediate parameter regimes (we used $V = 5.0$) by the absence of significant finite-size effects in the entanglement entropies [see Fig. 10(c), even for $L = 8$ (not shown)]. In

Appendix A 2, we work out the effective Hamiltonian up to second-order hopping processes (via one virtual state) and compare the predictions with exact diagonalization for $L = 8$. Because, furthermore, the excited domain-wall states are far below the bulk excitation gap of order U, we find a good agreement of the low-energy spectra.

Similarly, for the low V regime with boundary condition (C) in the limit $U \gg V, J$, appropriate states $|\psi_j\rangle$ are given by Eq. (14) with $d = L + 1$. These are not strictly domain-wall states, but fulfill the same role. However, the finite-size scaling of entanglement entropies [see Fig. 10(a)] indicates that here the assumption of width zero is not applicable in intermediate parameter regimes. Equation (10), representing domain-wall states in the HI phase, is an example of states that do not make this assumption.

2. Example for an effective domain-wall Hamiltonian

Here we work out in more detail the effective Hamiltonian on the reduced space of domain-wall states for the exemplary case of the DW phase with boundary condition (A even). We compare the results with exact diagonalization for $L = 8$ sites. As mentioned in the main text, in the limit $V \gg U \gg J$ the lowest-energy states in the occupation number basis are

$$|\psi_j\rangle = \underbrace{|20\ldots20\rangle}_{2(j-1)\text{ sites}} \otimes \underbrace{|02\ldots02\rangle}_{L-2(j-1)} \qquad j = 1, \ldots, \frac{L}{2} + 1, \tag{A4}$$

with energies $\approx LU/2$.

In order to obtain an effective Hamiltonian of the form of Eq. (A1) with nonzero tunneling between our basis states, we consider additional virtual states

$$|\varphi_l\rangle = \underbrace{|20\ldots20\rangle}_{2(l-1)\text{ sites}} \otimes |11\rangle \otimes \underbrace{|02\ldots02\rangle}_{L-2l} \qquad l = 1, \ldots, \frac{L}{2}, \tag{A5}$$

with energies separated from those of $|\psi_j\rangle$ by $V - U$. We only take into account the lowest-order process between $|\psi_j\rangle$ and $|\psi_{j+1}\rangle$, which involves two hoppings, i.e.,

$$|\psi_j\rangle \to |\varphi_j\rangle \to |\psi_{j+1}\rangle\,. \tag{A6}$$

The matrix elements of the Hamiltonian given by the states in Eqs. (A4) and (A5) are

$$\begin{aligned} H^a_{ij} &\equiv \langle\psi_i|\,\hat{H}\,|\psi_j\rangle = \frac{L}{2}U\delta_{ij}, \\ H^b_{ij} &\equiv \langle\varphi_i|\,\hat{H}\,|\varphi_j\rangle = \left[\left(\frac{L}{2} - 1\right)U + V\right]\delta_{ij}, \\ W_{ij} &\equiv \langle\varphi_i|\,\hat{H}\,|\psi_j\rangle = -\sqrt{2}J(\delta_{ij} + \delta_{i+1,j}). \end{aligned} \tag{A7}$$

Thus, the Hamiltonian in this subspace can be written as

$$\tilde{H} = \begin{pmatrix} H^a & W^T \\ W & H^b \end{pmatrix} \in \mathbb{R}^{(L+1)\times(L+1)}. \tag{A8}$$

When $J \ll U \ll V$, the domain-wall states $|\psi_j\rangle$ and the virtual states $|\varphi_j\rangle$ are hybridized by W, while $|\psi_j\rangle$ carry almost all the weight in the low-energy states. This permits a further restriction of the Hilbert space by ignoring $|\varphi_l\rangle$ (here we follow Chap. 3 of Ref. [33]). Using states $|a\rangle \in \text{span}\{|\psi_j\rangle\}$ and $|b\rangle \in \text{span}\{|\varphi_l\rangle\}$, the Schrödinger equation reads

$$\begin{aligned} H^a\,|a\rangle + W^T\,|b\rangle &= E\,|a\rangle\,, \\ W\,|a\rangle + H^b\,|b\rangle &= E\,|b\rangle\,. \end{aligned} \tag{A9}$$

Focusing on the lower energies $E \approx LU/2$, we can approximate

$$E\mathbb{1}_{\frac{L}{2}} - H^b \approx (U - V)\mathbb{1}_{\frac{L}{2}}. \tag{A10}$$

Then, by solving the second line of Eq. (A9) for $|b\rangle$ and inserting it into the first line, the effective Hamiltonian acting only on $|a\rangle$ attains the tridiagonal form

$$\begin{aligned} \hat{H}_{\text{eff}} &= H^a + \frac{1}{U - V}W^T W \\ &= \begin{pmatrix} D_{\text{edge}} & \tilde{J} & 0 & \cdots & 0 \\ \tilde{J} & D & \tilde{J} & \cdots & 0 \\ 0 & \tilde{J} & \ddots & & \vdots \\ \vdots & \vdots & & D & \tilde{J} \\ 0 & 0 & \cdots & \tilde{J} & D_{\text{edge}} \end{pmatrix} \end{aligned} \tag{A11}$$

with an effective tunneling parameter

$$\tilde{J} = 2\frac{J^2}{U - V} < 0 \tag{A12}$$

and renormalized diagonal elements

$$\begin{aligned} D_{\text{edge}} &= \frac{L}{2}U + 2\frac{J^2}{V - U}, \\ D &= \frac{L}{2}U + 4\frac{J^2}{V - U}. \end{aligned} \tag{A13}$$

Neglecting the L independent terms in Eq. (A13), which contain the influence of the edge on the domain-wall states, the effective Hamiltonian yields the form of Eq. (A1). The eigenvalues for this matrix form are known to be [32]

$$E_k = D + 2\tilde{J}\cos\left(\frac{\pi k}{\frac{L}{2} + 2}\right), k = 1, \ldots, \frac{L}{2} + 1. \tag{A14}$$

The eigenstates are given by $|k\rangle$ as in Eq. (A2).

A comparison of the exact low-energy band with the prediction of the effective theory confirms the qualitative dependence of the spectrum on V for $L = 8$ (see Fig. 11). This leads us to the conjecture that the spectrum of the DW phase with boundary conditions (A) is actually gapless; the elementary excitations are long-wavelength modes of the domain wall.

The effective theory does not give a good approximation of the energies for $V \lesssim 10 \approx 2U$ (see Fig. 11) and breaks down at $V = U$ due to diverging couplings $\tilde{J}$. However, our DMRG simulations in the previous sections for the DW phase with $V < U$ indicate that even in this region the ground state shows qualitatively the same correlations and occupation pattern as our effective theory. An extension of the effective theory by number fluctuations in the domain-wall basis states and higher-order hopping processes can in principle extend the region of applicability.

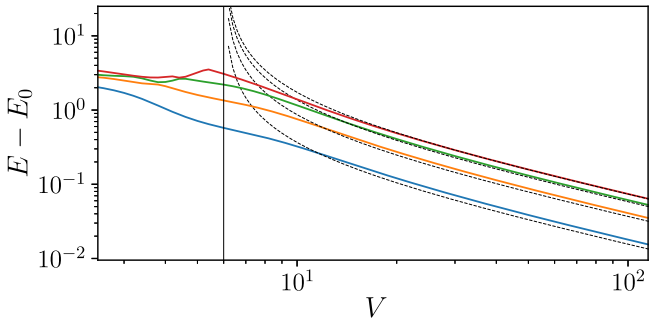

FIG. 11. Comparison of the exact low-energy band (solid lines) with the prediction of the effective theory (dashed lines) for $U = 6$ and $L = 8$. Energies are measured relative to the ground-state energy E_0.

APPENDIX B: BOUNDARY CONDITIONS (B) AND (C) WITH ODD SYSTEM SIZES

As in the case of boundary condition (A), for boundary conditions (B) and (C) we only see a difference between even and odd L in the DW phase. In Fig. 12 we plot occupation patterns and the density-density correlation function for $U = 6$ and $V = 5$. We use a smaller system size than in the main text ($L = 101$), so that it is easier to see the occupations of the edges. Comparing (B odd) [see Figs. 12(a) and 12(c)] with (B even), the only essential difference lies at the left edge, where we apply a positive chemical potential; the occupation number at this edge is close to 1, whereas for (B even) it is much smaller than 1. Thus, effectively, the domain wall of the case (A odd), described by the states

$$|20\ldots20102\ldots02\rangle\,, \tag{B1}$$

has moved to the edge:

$$|10202\ldots02\rangle\,. \tag{B2}$$

Our interpretation is that the chemical potentials of strength $\mu = 2J$ are still weaker than the nearest-neighbor repulsion of strength $V = 5J$, bringing the ($n = 1$) site to the edge, but not forcing $n = 0$.

On the other hand, the case (C odd) [see Figs. 12(b) and 12(d)] can be effectively understood by inserting a single particle into the domain wall of (A odd) shown in Eq. (B1), which yields

$$|20\ldots20202\ldots02\rangle\,. \tag{B3}$$

Thus there is no domain wall at all and no sign flip of the correlation functions, which are present in the even case.

APPENDIX C: OVERLAPS AND SUPERFLUID CORRELATIONS OF THE HI TOY STATES

Here we show some details of the calculation of the superfluid correlation function using the toy states for the HI phase with a domain wall:

$$|\psi_j\rangle = \hat{a}_1^\dagger \prod_{i=1}^{j-1}(\hat{a}_i^\dagger + \hat{a}_{i+1}^\dagger) \prod_{i=j+1}^{L-1}(\hat{a}_i^\dagger + \hat{a}_{i+1}^\dagger)\hat{a}_L^\dagger\,|0\rangle\,. \tag{C1}$$

For a ground state $|G\rangle = \sum_j w_j\,|\psi_j\rangle\,/\sqrt{|\,\langle\psi_j|\psi_j\rangle\,|}$, the correlation function reads

$$\langle a_i^\dagger a_j\rangle = \sum_{k,l} w_k w_l \frac{\langle\psi_k|a_i^\dagger a_j|\psi_l\rangle}{\sqrt{|\,\langle\psi_k|\psi_k\rangle\,|}\sqrt{|\,\langle\psi_l|\psi_l\rangle\,|}}, \tag{C2}$$

where the normalization factor is included in the denominator. Thus, we need to calculate overlaps of the forms $\langle\psi_k|\psi_l\rangle$ and $\langle\psi_k|\,\hat{a}_i^\dagger\hat{a}_j\,|\psi_l\rangle$.

In order to obtain these quantities, notice that the basis states $|\psi_j\rangle$ in Eq. (C1) are products of a state on the left j sites and a state on the right $L - j$ sites. As mentioned in the main text, the extra site occupations $\delta n = n - 1$ of the left (right) part close to the sites 1 and j ($j + 1$ and L) sum up to $+1/2$ and $-1/2$ ($-1/2$ and $+1/2$). This corresponds to topological edge states and is very similar to the spin-1/2 degrees of freedom at the edges of the Affleck-Kennedy-Lieb-Tasaki chain [30]. With this in mind, we denote the basis states as

$$|\psi_j\rangle = |{+}{-}\rangle_{(j)} \otimes |{-}{+}\rangle_{(L-j)}\,, \tag{C3}$$

where we have introduced

$$|{+}{-}\rangle_{(n)} = \hat{a}_1^\dagger \prod_{i=1}^{n-1}(\hat{a}_i^\dagger + \hat{a}_{i+1}^\dagger)\,|0\rangle\,,$$

$$|{-}{+}\rangle_{(n)} = \prod_{i=1}^{n-1}(\hat{a}_i^\dagger + \hat{a}_{i+1}^\dagger)\hat{a}_n^\dagger\,|0\rangle\,. \tag{C4}$$

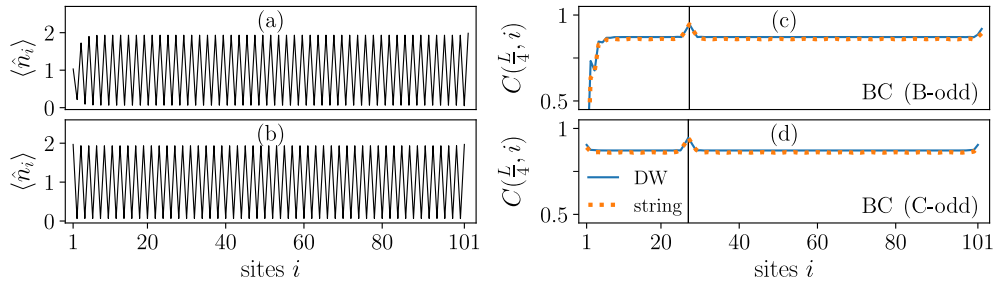

FIG. 12. Boundary conditions (B) [top row] and (C) [bottom row] for $L = 101$, $U = 6$, and $V = 5.0$ (corresponding to the DW phase). The left panels (a) and (b) depict the occupation patterns. The right panels (c) and (d) show the string (dashed orange) and DW (solid blue) correlation function $C_{\mathrm{DW}}(L/4, i)$. Vertical lines indicate the maxima at $L/4$.

In this notation, the signs $\pm$ refer to the edge degrees of freedom and the subscript n is the length of the chain, on which the vacuum $|0\rangle$ lives. For completeness and later use, one should also introduce the symmetric states

$$|--\rangle_{(n)} = \prod_{i=1}^{n-1}(\hat{a}_i^\dagger + \hat{a}_{i+1}^\dagger)\,|0\rangle\,,$$
$$|++\rangle_{(n)} = \hat{a}_1^\dagger \prod_{i=1}^{n-1}(\hat{a}_i^\dagger + \hat{a}_{i+1}^\dagger)\hat{a}_n^\dagger\,|0\rangle\,, \tag{C5}$$

and recognize that for any combination $\sigma_1, \sigma_n = \pm$ of edge states and any $1 < m < n$

$$|\sigma_1, \sigma_n\rangle_{(n)} = |\sigma_1 +\rangle_{(m)} \otimes |-\sigma_n\rangle_{(n-m)} + |\sigma_1 -\rangle_{(m)} \otimes |+\sigma_n\rangle_{(n-m)}\,. \tag{C6}$$

The next step is to calculate the overlaps of these building blocks, for which it is useful to introduce the following variation of the Fibonacci sequence:

$$P_{ab}(n) = 2P_{ab}(n-1) + P_{ab}(n-2),$$
$$P_{ab}(0) = a,\ P_{ab}(1) = b. \tag{C7}$$

We note that these grow approximately in an exponential fashion. For the cases $a = 1$, $b \in \{0, 1\}$, which occur below, the well-known explicit form is given by

$$P_{11}(n) = \left(\frac{(1+\sqrt{2})^n}{2} + \frac{(1-\sqrt{2})^n}{2}\right) \overset{n\gg 1}{\approx} \frac{(1+\sqrt{2})^n}{2},$$
$$P_{01}(n) = \left(\frac{(1+\sqrt{2})^n}{2\sqrt{2}} - \frac{(1-\sqrt{2})^n}{2\sqrt{2}}\right) \overset{n\gg 1}{\approx} \frac{(1+\sqrt{2})^n}{2\sqrt{2}}. \tag{C8}$$

By a recursive procedure, it can be shown that the nonzero overlaps are

$$_{(n)}\langle + - | + -\rangle_{(n)} = {}_{(n)}\langle - + | - +\rangle_{(n)} = P_{11}(n),$$
$$\frac{{}_{(n)}\langle + + | + +\rangle_{(n)}}{2} = {}_{(n)}\langle - - | - -\rangle_{(n)} = P_{01}(n),$$
$$_{(n)}\langle + - | - +\rangle_{(n)} = 1. \tag{C9}$$

All other combinations vanish, because the states differ in the total particle number, for instance, $|++\rangle_{(n)} = \hat{a}_1^\dagger\,|-+\rangle_{(n)}$.

Combining Eqs. (C3), (C6),(C8), and (C9), and assuming $k < l$ without loss of generality, it follows that the overlap of two normalized domain-wall basis states $|\psi_k\rangle / \sqrt{\langle\psi_k|\psi_k\rangle}$ is given by

$$\frac{\langle\psi_k|\psi_l\rangle}{\sqrt{|\,\langle\psi_k|\psi_k\rangle\,|}\sqrt{|\,\langle\psi_l|\psi_l\rangle\,|}} = \frac{P_{11}(k)P_{11}(L-l)}{\sqrt{P_{11}(k)P_{11}(L-k)}\sqrt{P_{11}(l)P_{11}(L-l)}} \approx (1+\sqrt{2})^{-|k-l|} \equiv e^{-\xi|k-l|}. \tag{C10}$$

This shows that these overlaps decay roughly exponentially with decay length $\xi = [\ln(1+\sqrt{2})]^{-1} \approx 1.3$.

For the SF correlation function, we use the fact that (assuming $k+1 < j$ without significant loss of generality)

$$\hat{a}_j\,|\psi_k\rangle = |+-\rangle_{(k)} \otimes |--\rangle_{[(j-1)-k]} \otimes |-+\rangle_{[L-(j-1)]} + |+-\rangle_{(k)} \otimes |--\rangle_{(j-k)} \otimes |-+\rangle_{(L-j)} \equiv |\psi_{k,j-1}\rangle + |\psi_{k,j}\rangle\,, \tag{C11}$$

which means that the annihilation operator creates another domain wall at the bonds $(j-1, j)$ and $(j, j+1)$, denoted by a second subscript. The cases $j = k, k+1$ are slightly different, but we omit them for brevity.

Using Eq. (C11), the SF correlation function is calculated in the same way as the overlap in Eq. (C10). Essentially, it is given by terms of the form (assuming $k < l < j < i$)

$$\frac{\langle\psi_{k,j}|\psi_{l,i}\rangle}{\sqrt{|\,\langle\psi_{k,j}|\psi_{k,j}\rangle\,|}\sqrt{|\,\langle\psi_{l,i}|\psi_{l,i}\rangle\,|}} = \frac{P_{11}(k)P_{01}(j-l)P_{11}(L-i)}{\sqrt{P_{11}(k)P_{01}(j-k)P_{11}(L-j)}\sqrt{P_{11}(l)P_{01}(i-l)P_{11}(L-i)}} \approx (1+\sqrt{2})^{-(|k-l|+|j-i|)} \equiv e^{-\xi(|k-l|+|j-i|)}, \tag{C12}$$

These terms vanish, if $\max(k, j) < \min(l, i)$ or $\max(l, i) < \min(k, j)$. A plateau value of the SF correlation that is similar to the one calculated by DMRG is obtained by replacing the exact formula by the exponential form and setting $\xi \approx 4$.

APPENDIX D: ENTANGLEMENT ENTROPY OF THE DOMAIN-WALL STATE

In Sec. IV we have compared entanglement entropies that were calculated by DMRG with the sum of a bulk contribution and a generic domain-wall contribution. Here we derive the formulas of Eqs. (20) and (21) in the thermodynamic limit. As in Secs. IV and Appendix A, let $|\psi_j\rangle$ $[j = 1, \ldots, d = O(L)]$ denote generic domain-wall states of finite width, i.e., $\langle\psi_i|\psi_j\rangle \to 0$ for $|i-j| \to \infty$. We want to calculate the domain-wall entropy for the bipartition at site l. For simplicity, let us first assume that the basis states can be written in a product form:

$$|\psi_j\rangle = \begin{cases} |L_j\rangle \otimes |R_1\rangle & \text{for } j < m_l \\ |L_{m_l}\rangle \otimes |R_{j-m_l+1}\rangle & \text{for } j \geqslant m_l. \end{cases}, \tag{D1}$$

where $|L_j\rangle$ ($|R_j\rangle$) represent states on the left (right) block of the chain. The domain wall lies to the left of site l for $j < m_l$, and otherwise to the right. For instance, with the states from Appendix A 2, this means

$$|L_j\rangle \otimes |R_1\rangle = |20\ldots20\rangle\,|02\ldots02\rangle \otimes |02\ldots02\rangle\,,$$
$$|L_{m_l}\rangle \otimes |R_{j-m_l+1}\rangle = |20\ldots20\rangle \otimes |20\ldots20\rangle\,|02\ldots02\rangle\,, \tag{D2}$$

where the domain wall is understood to lie between the sites $2j-2$ and $2j-1$.

If the coefficient of $|\psi_j\rangle$ in the ground state $|G\rangle$ is $\propto w_j$ (e.g., corresponding to the sinelike wave function derived in Appendix A 1), the weight of the domain-wall states in the left block in the ground state is

$$p_l = \sum_{j<m_l} |\,\langle\psi_j|G\rangle\,|^2 = N^{-1}\sum_{j<m_l} w_j^2\,, \quad N = \sum_j w_j^2. \tag{D3}$$

With this, we can define normalized states on the left and right subsystem

$$|\tilde{L}\rangle = \frac{1}{\sqrt{p_l N}} \sum_{j<m_l} w_j |L_j\rangle ,$$
$$|\tilde{R}\rangle = \frac{1}{\sqrt{(1-p_l)N}} \sum_{j\geqslant m_l} w_j |R_{j-m_l+1}\rangle , \tag{D4}$$

adding up the states in each of the two cases of Eq. (D1), and express the ground state as

$$\begin{aligned} |G\rangle &= N^{-\frac{1}{2}} \sum_{j=1}^{d} w_j |\psi_j\rangle \\ &= N^{-\frac{1}{2}} \left(\sum_{j<m_l} w_j |L_j\rangle |R_1\rangle + \sum_{j\geqslant m_l} w_j \left|L_{m_l}\right\rangle |R_{j-m_l+1}\rangle \right) \\ &= \sqrt{p_l}\, |\tilde{L}\rangle |R_1\rangle + \sqrt{1-p_l}\, \left|L_{m_l}\right\rangle |\tilde{R}\rangle . \end{aligned} \tag{D5}$$

Assuming that the basis states are orthogonal, i.e., $\langle\psi_i|\psi_j\rangle = \delta_{ij}$, the reduced density matrix of the left block simplifies to

$$\begin{aligned} \rho_l &= \mathrm{tr}_{>l}\{|G\rangle\langle G|\} \\ &= \sum_{j\geqslant m_l} \left\langle R_{j-m_l+1}\middle|G\right\rangle \left\langle G\middle|R_{j-m_l+1}\right\rangle \\ &= p_l\, |\tilde{L}\rangle\langle\tilde{L}| + (1-p_l) \left|L_{m_l}\right\rangle\left\langle L_{m_l}\right| \\ &\quad + \left(\frac{w_{m_l}}{N}\right)^2 \left(|\tilde{L}\rangle \left\langle L_{m_l}\right| + \left|L_{m_l}\right\rangle \langle\tilde{L}| \right), \end{aligned} \tag{D6}$$

where the off-diagonal elements come exclusively from the terms $|\tilde{L}\rangle|R_1\rangle$ and $|L_{m_l}\rangle|R_1\rangle$. In Appendix E, in Eq. (E2) we see a simple example for a case where the last term is absent, and in Eq. (E1) an example where it is present.

Taking the thermodynamic limit $L, d \to \infty$ with fixed l/L and m_l/d, we have $w_l/N \to 0$ and thus the reduced density matrix becomes diagonal:

$$\rho_l \xrightarrow{L\to\infty} p_l\, |\tilde{L}\rangle\langle\tilde{L}| + (1-p_l) \left|L_{m_l}\right\rangle\left\langle L_{m_l}\right| . \tag{D7}$$

This obviously gives the domain-wall entropy shown in Eq. (20). If we do not assume orthogonality, there are larger off-diagonal contributions, due to $\langle R_1|R_{j-m_l+1}\rangle \neq 0$, causing finite-size effects as in Figs. 10(a) and 10(c). However, these are negligible in the thermodynamic limit.

If we do not assume the product form of Eq. (D1), we have to write the states as a Schmidt decomposition:

$$|\psi_j\rangle = \begin{cases} \sum_\alpha \lambda_j^\alpha \left|L_j^\alpha\right\rangle \otimes \left|R_1^\alpha\right\rangle & \text{for } j < m_l \\ \sum_\alpha \lambda_j^\alpha \left|L_{m_l}^\alpha\right\rangle \otimes \left|R_{j-m_l+1}^\alpha\right\rangle & \text{for } j \geqslant m_l . \end{cases} \tag{D8}$$

where $\{(\lambda_j^\alpha)^2 : \alpha\}$ is the entanglement spectrum of the bipartition of $|\psi_j\rangle$ at site l. For $|j-m_l|$ sufficiently large, i.e., when the domain wall is sufficiently far from site l, this corresponds to the entanglement spectrum of the underlying bulk phase ($\lambda_j^\alpha \to \lambda^\alpha$). Going through the same calculation as above and ignoring contributions where the domain wall is close to l (as the corresponding weights w_j/N vanish in the thermodynamic limit), we first define

$$|\tilde{L}^\alpha\rangle = \frac{1}{\sqrt{p_l N}} \sum_{j<m_l} w_j \left|L_j^\alpha\right\rangle ,$$
$$|\tilde{R}^\alpha\rangle = \frac{1}{\sqrt{(1-p_l)N}} \sum_{j\geqslant m_l} w_j \left|R_{j-m_l+1}^\alpha\right\rangle , \tag{D9}$$

and then arrive at

$$\rho_l \xrightarrow{L\to\infty} p_l \sum_\alpha \lambda^\alpha |\tilde{L}^\alpha\rangle\langle\tilde{L}^\alpha| + (1-p_l) \sum_\alpha \lambda^\alpha \left|L_{m_l}^\alpha\right\rangle\left\langle L_{m_l}^\alpha\right| . \tag{D10}$$

From this it follows that the entropy can be written as

$$\begin{aligned} S &= -\sum_\alpha p_l\lambda^\alpha \ln(p_l\lambda^\alpha) + (1-p_l)\lambda^\alpha \ln[(1-p_l)\lambda^\alpha] \\ &= -\sum_\alpha \lambda^\alpha \ln(\lambda^\alpha) - p_l \ln(p_l) - (1-p_l)\ln(1-p_l). \end{aligned} \tag{D11}$$

The first term is the entropy of the underlying bulk phase, while the rest give the domain-wall contribution. This explains the results from Sec. IV.

APPENDIX E: ENTANGLEMENT SPECTRA

As a supplement to our analysis of entanglement entropies in Sec. IV, here we show the most significant values of the full entanglement spectra for the symmetric bipartition at $L/2$. First, this offers a closer look at the system size dependence. Second, we can study degeneracies; in particular, the HI phase is known to have a doubly degenerate entanglement spectrum [10,21]. This is a footprint of the HI being a so-called symmetry-protected topological phase: as long as a certain symmetry of the Hamiltonian (e.g., lattice inversion for the HI phase) is not broken by a change of its parameters, the degeneracies can only be removed through a phase transition.

In the present case, we have to deal with an additional, trivial type of degeneracy due to the fact that lattice inversion symmetry is present in all ground states. Let ρ_l denote the block of the reduced density matrix of the left half of the system with particle number l. As a consequence of the inversion symmetry, the blocks fulfill the relation $\rho_l = \rho_{L-l}$ [21]. For total particle number $N = L$, as in the case of the boundary conditions (A), this implies a partial double degeneracy of the entanglement spectrum. Only the block $\rho_{L/2}$ does not have any degenerate counterpart. On the other hand, for boundary condition (C) with $N = L+1$ we have a complete double degeneracy, because the block $\rho_{L/2} = \rho_{L/2+1}$ now has a counterpart. With boundary condition (B), where we used edge potentials to break the inversion symmetry, we do not expect such degeneracies.

In Fig. 13 we show entanglement spectra for boundary condition (A even), (B), and (C), respectively. Each of the figures contains data on one ground state in the MI ($V = 1.0$), HI ($V = 3.7$), and DW ($V = 5.0$). The first things we note are the partial double degeneracy with boundary condition (A) [first column] and the complete double degeneracy with boundary condition (C) [third column], which are present independently of the phase. These degeneracies are due to the block symmetry described above. In addition, in the DW

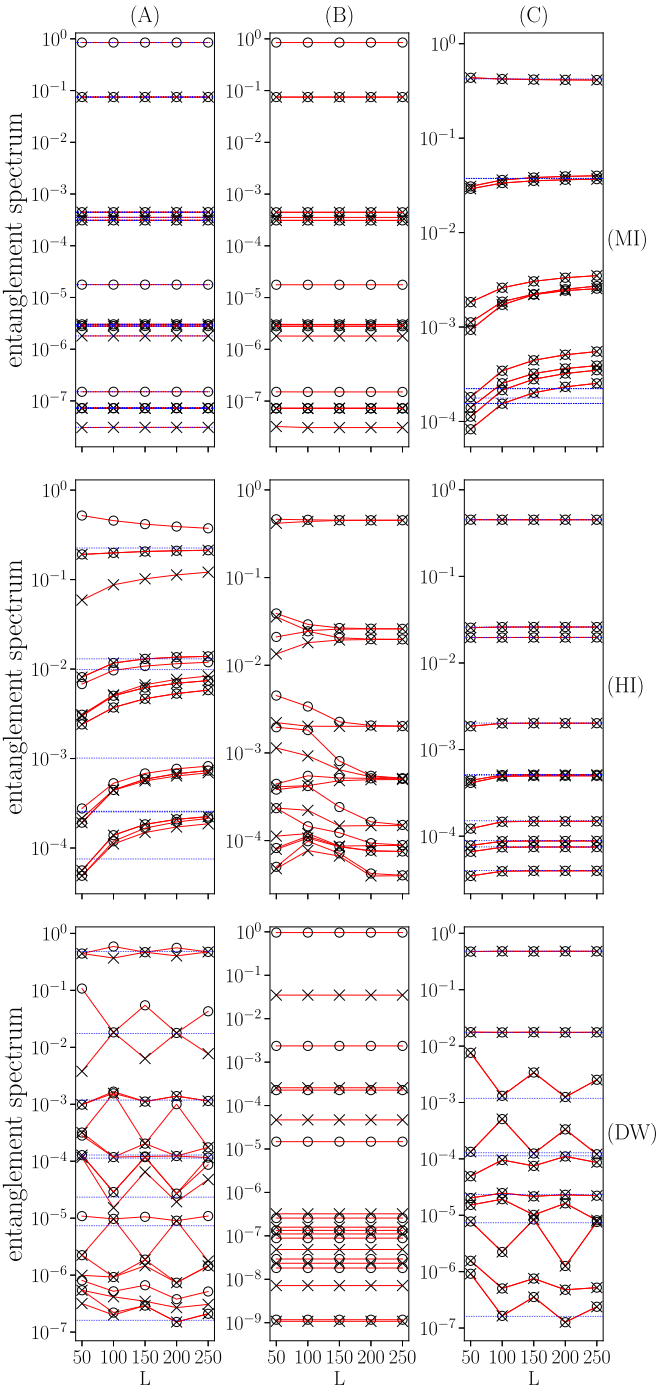

FIG. 13. Finite-size scaling of the 20 largest values of the entanglement spectra. Columns correspond to boundary condition (A), (B), and (C). Rows represent points deep in the MI ($V = 1.0$), HI ($V = 3.7$), and DW ($V = 5.0$) phases. Dotted blue lines indicate the bulk values from (B) for MI-(A) and HI-(C) and half those values otherwise. Circles and crosses as labels alternate as an aid to the eye.

phase of BC (A) the values of the entanglement spectrum oscillate (see bottom left panel). For the largest two eigenvalues, this can be understood in terms of the effective picture described in Appendix A 2: If L is divisible by 4, the basis states can decomposed as

$$\begin{aligned} &\underbrace{|20\ldots20\rangle}_{L/2\text{ particles}}\,\underbrace{|02\ldots02\rangle}_{L/2\text{ particles}} \otimes \underbrace{|02\ldots02\rangle}_{L/2\text{ particles}}, \\ &\underbrace{|20\ldots20\rangle}_{L/2\text{ particles}} \otimes \underbrace{|20\ldots20\rangle\,|02\ldots02\rangle}_{L/2\text{ particles}}, \end{aligned} \tag{E1}$$

where the $\otimes$ sign indicates the middle of the chain and the domain wall is either on the left (upper line) or the right (lower line) of the middle. If L is not divisible by 4, the basis states are decomposed as

$$\begin{aligned} &\underbrace{|20\ldots20\rangle\,|02\ldots020\rangle}_{L/2-1\text{ particles}} \otimes \underbrace{|202\ldots02\rangle}_{L/2+1\text{ particles}} \\ &\underbrace{|20\ldots202\rangle}_{L/2+1\text{ particles}} \otimes \underbrace{|020\ldots20\rangle\,|02\ldots02\rangle}_{L/2-1\text{ particles}}. \end{aligned} \tag{E2}$$

In the case of Eq. (E2), these states give two degenerate contributions $\rho_{L/2\pm1}$ to the reduced density matrix. Equation (E1) makes only one contribution $\rho_{L/2}$, which does not imply degeneracies.

We note that the entanglement spectrum converges in L for boundary condition (B) [middle column]. We consider these to be the bulk values. Here, despite the explicitly broken inversion symmetry, the HI is characterized by a double degeneracy and the MI is characterized by a partial double degeneracy. A comparison with boundary conditions (A) and (C) shows that in cases with no domain wall the values coincide [i.e., MI with (A) and HI with (C)]. On the other hand, if there is a domain wall [i.e., MI with (C), HI with (A), DW for both (A) and (C)], many values converge slowly in the system size (we checked this to be consistent with a power law, not shown). In these cases, the thermodynamic limit is consistent with half the bulk value, which implies the behavior of entanglement entropies found in Sec. IV (see blue lines in Fig. 13). In particular, the largest value of the sign-flipping HI with boundary condition (A) appears to be fourfold instead of twofold degenerate at half the bulk value in the thermodynamic limit. This can be understood as a combination of the topologically protected double degeneracy and the influence of the domain wall. One exception is the values below the sixth largest in the MI with boundary condition (C), where the extra boson is delocalized. These do not have a counterpart in the bulk spectrum.

[1] I. Bloch, Nat. Phys. **1**, 23 (2005).
[2] M. Lewenstein, A. Sanpera, V. Ahufinger, B. Damski, A. Sen(De), and U. Sen, Adv. Phys. **56**, 243 (2007).
[3] D. Jaksch and P. Zoller, Ann. Phys. (NY) **315**, 52 (2005).
[4] T. Lahaye, C. Menotti, L. Santos, M. Lewenstein, and T. Pfau, Rep. Prog. Phys. **72**, 126401 (2009).
[5] S. Baier, M. J. Mark, D. Petter, K. Aikawa, L. Chomaz, Z. Cai, M. Baranov, P. Zoller, and F. Ferlaino, Science **352**, 201 (2016).

[6] T. D. Kühner, S. R. White, and H. Monien, Phys. Rev. B **61**, 12474 (2000).
[7] E. G. Dalla Torre, E. Berg, and E. Altman, Phys. Rev. Lett. **97**, 260401 (2006).
[8] E. Berg, E. G. Dalla Torre, T. Giamarchi, and E. Altman, Phys. Rev. B **77**, 245119 (2008).
[9] S. Ejima, F. Lange, and H. Fehske, Phys. Rev. Lett. **113**, 020401 (2014).
[10] F. Pollmann, A. M. Turner, E. Berg, and M. Oshikawa, Phys. Rev. B **81**, 064439 (2010).
[11] C. Muldoon, L. Brandt, J. Dong, D. Stuart, E. Brainis, M. Himsworth, and A. Kuhn, New J. Phys. **14**, 073051 (2012).
[12] D. Jaschke, M. L. Wall, and L. D. Carr, Comput. Phys. Commun. **225**, 59 (2017).
[13] P. M. Chaikin and T. C. Lubensky, *Principles of Condensed Matter Physics* (Cambridge University, Cambridge, England, 1995).
[14] E. G. Dalla Torre, J. Phys. B **46**, 085303 (2013).
[15] D. Rossini and R. Fazio, New J. Phys. **14**, 065012 (2012).
[16] G. G. Batrouni, R. T. Scalettar, V. G. Rousseau, and B. Grémaud, Phys. Rev. Lett. **110**, 265303 (2013).
[17] G. G. Batrouni, V. G. Rousseau, R. T. Scalettar, and B. Grémaud, Phys. Rev. B **90**, 205123 (2014).
[18] G. G. Batrouni, V. G. Rousseau, R. T. Scalettar, and B. Grémaud, J. Phys. Conf. Ser. **640**, 012042 (2015).
[19] C. Kollath, G. Roux, G. Biroli, and A. M. Läuchli, J. Stat. Mech. Theor. Exp. (2010) P08011.
[20] B. Grémaud and G. G. Batrouni, Phys. Rev. B **93**, 035108 (2016).
[21] X. Deng and L. Santos, Phys. Rev. B **84**, 085138 (2011).
[22] K. zu Münster, F. Gebhard, S. Ejima, and H. Fehske, Phys. Rev. A **89**, 063623 (2014).
[23] J. M. Kurdestany, R. V. Pai, S. Mukerjee, and R. Pandit, arXiv:1403.2315 (2014).
[24] C. N. Yang, Rev. Mod. Phys. **34**, 694 (1962).
[25] M. Lewenstein, A. Sanpera, and V. Ahufinger, *Ultracold Atoms in Optical Lattices* (Oxford University, New York, 2012).
[26] W. Xiao-Gang, *Quantum Field Theory of Many-Body Systems: From the Origin of Sound to an Origin of Light and Electrons* (Oxford University, New York, 2007).
[27] P. Calabrese and J. Cardy, J. Stat. Mech. Theor. Exp. (2004) P06002.
[28] H. J. Mikeska and A. K. Kolezhuk, Lect. Notes Phys. **645**, 1 (2004).
[29] T. Kennedy and H. Tasaki, Commun. Math. Phys. **147**, 431 (1992).
[30] I. Affleck, T. Kennedy, E. H. Lieb, and H. Tasaki, Commun. Math. Phys. **115**, 477 (1988).
[31] M. Soriano and J. J. Palacios, Phys. Rev. B **90**, 075128 (2014).
[32] O. Toeplitz, Math. Ann. **70**, 351 (1911).
[33] A. Auerbach, *Interacting Electrons and Quantum Magnetism* (Springer-Verlag, Berlin, 1994).